Published in final edited form as:

Cell Rep. 2018 June 26; 23(13): 3759–3768. doi:10.1016/j.celrep.2018.05.096.

NMDA Receptor Autoantibodies in Autoimmune Encephalitis Cause a Subunit-Specific Nanoscale Redistribution of NMDA Receptors

Laurent Ladépêche[1,2,9,*], **Jesús Planagumà**[1,2,9], **Shreyasi Thakur**[1,5], **Irina Suárez**[1,7], **Makoto Hara**[2,8], **Joseph Steven Borbely**[1], **Angel Sandoval**[1], **Lara Laparra-Cuervo**[1], **Josep Dalmau**[2,3,4,6,10], and **Melike Lakadamyali**[1,5,10,11,*]

[1]ICFO-Institut de Ciències Fotòniques, The Barcelona Institute of Science and Technology, 08860 Castelldefels (Barcelona), Spain

[2]Institut d'Investigacions Biomèdiques August Pi i Sunyer (IDIBAPS), Hospital Clínic c/Villarroel 170, 08036 Barcelona, Spain

[3]Department of Neurology, University of Pennsylvania, Philadelphia, PA 19104, USA

[4]Catalan Institution for Research and Advanced Studies (ICREA), 08010 Barcelona, Spain

[5]Department of Physiology, Perelman School of Medicine, University of Pennsylvania, 700 Clinical Research Building, 415 Curie Boulevard, Philadelphia, PA 19104-6085, USA

[6]Centro de Investigación Biomédica en Red de Enfermedades Raras (CIBERER), Av. Monforte de Lemos, 3-5. Pabellón 11. Planta 0, 28029 Madrid, Spain

SUMMARY

Anti-N-methyl-D-aspartate receptor (NMDAR) encephalitis is a severe neuropsychiatric disorder mediated by autoantibodies against the GluN1 subunit of the NMDAR. Patients' antibodies cause crosslinking and internalization of NMDAR, but the synaptic events leading to depletion of NMDAR are poorly understood. Using super-resolution microscopy, we studied the effects of the autoantibodies on the nanoscale distribution of NMDAR in cultured neurons. Our findings show

[*]Correspondence: laurent.ladepeche@icfo.eu (L.L.), melikel@pennmedicine.upenn.edu (M.L.).
[7]Present address: Institute for Cardiovascular Organogenesis and Regeneration, Faculty of Medicine, WWU Münster, 48149 Münster, Germany
[8]Present address: Division of Neurology, Department of Medicine, Nihon University School of Medicine, Tokyo, Japan
[9]These authors contributed equally
[10]Senior author
[11]Lead Contact

SUPPLEMENTAL INFORMATION

Supplemental Information includes Supplemental Experimental Procedures, six figures, one table, and three videos and can be found with this article online at https://doi.org/10.1016/j.celrep.2018.05.096.

AUTHOR CONTRIBUTIONS

L.L., J.P., J.D., and M.L. designed the experiments and data analysis. L.L., J.P., I.S., M.H., and L.L.-C. performed the experiments and data analysis. S.T. designed, ran, and analyzed the Monte Carlo simulations. J.S.B. wrote the software for data analysis. A.S. labeled the antibodies for STORM. M.L., L.L., J.P., and J.D. wrote the manuscript. All authors provided feedback on the manuscript. M.L. and J.D. supervised the project.

DECLARATION OF INTERESTS

J.D. holds a patent for the use of Ma2 and NMDAR as an autoantibody test, receives royalties related to this test, and has an unrestricted research grant from Euroimmun.

that, under control conditions, NMDARs form nanosized objects and patients' antibodies increase the clustering of synaptic and extrasynaptic receptors inside the nano-objects. This clustering is subunit specific and predominantly affects GluN2B-NMDARs. Following internalization, the remaining surface NMDARs return to control clustering levels but are preferentially retained at the synapse. Monte Carlo simulations using a model in which antibodies induce NMDAR cross-linking and disruption of interactions with other proteins recapitulated these results. Finally, activation of EphB2 receptor partially antagonized the antibody-mediated disorganization of the nanoscale surface distribution of NMDARs.

In Brief

Ladépêche et al. visualize NMDAR nanoorganization in a model of NMDAR encephalitis. NMDARs organize in nanoobjects, which show a time-dependent and subunit-specific change in their size and content upon patients' antibody treatment. EphB2 receptor activation, which stabilizes NMDAR-protein interactions, partially antagonizes the alteration of NMDAR nano-organization caused by patients' antibodies.

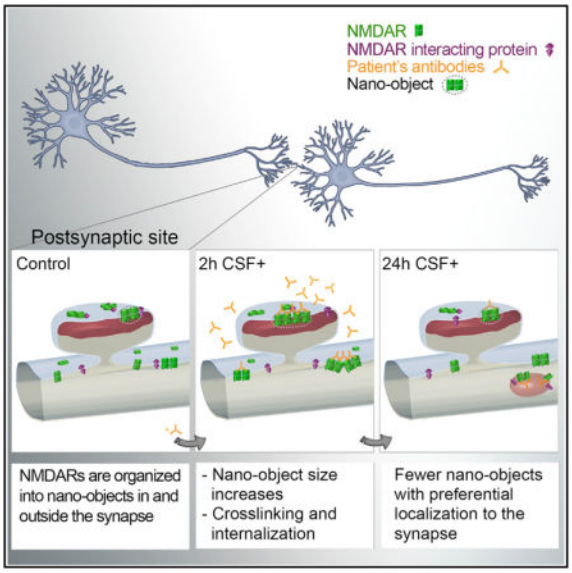

INTRODUCTION

The N-methyl-D-aspartate receptors (NMDARs) play a critical role in neuronal synaptic plasticity, a cellular correlate for learning and memory processes. NMDARs are heterotetramers mainly comprising two obligatory GluN1 subunits and two GluN2 subunits, of which GluN2A and GluN2B are the main subunits present in the hippocampus (Paoletti, 2011). Anti-NMDAR encephalitis is a recently identified autoimmune synaptopathy characterized by changes in behavior, psychosis, decrease of memory, seizures, stereotyped movements, autonomic instability, and coma (Dalmau and Graus, 2018). These symptoms are accompanied by the presence of autoantibodies in cerebrospinal fluid (CSF) and serum against extracellular epitopes of the GluN1 subunit of the NMDAR (Gleichman et al., 2012).

In cultured neurons and in an animal model of cerebroventricular transfer of patients' CSF, the autoantibodies altered the cell-surface dynamics of the NMDAR, causing their internalization, and decreased the NMDAR-dependent currents and synaptic plasticity, resulting in memory and behavioral alterations (Hughes et al., 2010; Mikasova et al., 2012; Moscato et al., 2014; Planagumà et al., 2015). In these studies, treatment with patients' antibodies caused a disruption of normal surface diffusion of the NMDAR, followed by their internalization. In contrast to these prominent effects on NMDARs, patients' antibodies did not alter the localization or expression of other glutamate receptors or synaptic proteins, number of synapses, dendritic spines, dendritic complexity, or cell survival (Hughes et al., 2010). Moreover, removal of patients' antibodies led to recovery of NMDAR levels, synaptic function, memory, and behavior. Other studies showed that activation of Ephrin-B2 (EphB2) receptor partially antagonized all pathogenic effects of patients' autoantibodies (Mikasova et al., 2012; Planagumà et al., 2016). Yet the time course of the changes of NMDAR distribution that take place at the synaptic level is unknown. Studies have shown that the nanoscale distribution and mobility of synaptic receptors, including NMDARs, are critical for normal neurotransmission (Dupuis et al., 2014; MacGillavry et al., 2013; Nair et al., 2013; Pennacchietti et al., 2017; Specht et al., 2013). Therefore, we reasoned that an antibody-mediated disruption of the NMDAR should also alter the nanoscale distribution of these receptors and synaptic function.

In the current study, we used a combination of biochemical approaches, confocal microscopy, super-resolution microscopy, and Monte Carlo simulations to determine the dynamic changes at the nanoscale level that lead to antibody-mediated reduction of surface NMDARs. We show that NMDARs are organized into small clusters or nano-objects inside the synapse and this nanoscale organization of NMDARs is disrupted in a subunit-dependent manner by patients' NMDAR autoantibodies.

RESULTS

Patients' Antibodies Induce Reorganization of Surface NMDAR at the Nanoscale Level

Using cultured hippocampal neurons, we first confirmed that the NMDAR antibodies present in patients' CSF caused internalization of surface NMDARs (Figure S1) (Hughes et al., 2010; Moscato et al., 2014). To determine the events that take place at the synapse leading to this decrease of surface NMDAR levels, we used single-molecule localization microscopy, in particular stochastic optical reconstruction microscopy (STORM) (Oddone et al., 2014; Rust et al., 2006). STORM revealed that under control conditions (neurons cultured in the presence of CSF without NMDAR antibodies), the NMDARs are organized in nanosized clusters along the dendrite (Figure 1A), which we refer to as nano-objects. Using a previously developed cluster analysis algorithm (Ricci et al., 2015), these nano-objects were automatically segmented, revealing their size and receptor content at the nanoscale level (Figure 1A).

Treatment of living cultured neurons with patients' NMDAR antibodies for different times showed a reduction in the number of surface NMDAR nano-objects per unit length of dendrite, reaching a plateau at 24 hr and displaying overall dynamics similar to those described in studies using confocal microscopy (Figure 1B; Figure S1) (Moscato et al.,

2014). To investigate the effect of patients' antibodies on synaptic distribution, size, and receptor content of NMDAR nano-objects, we performed dual-color STORM experiments by co-labeling NMDAR and PSD95, a protein of the postsynaptic density (PSD) known to interact with and stabilize the NMDARs at the synapse (Figure 2A). We measured the nearest-neighbor distances (NNDs) between NMDAR and PSD95 nano-objects, the NMDAR nano-object size, and the number of localizations per NMDAR nano-object, which is proportional to the relative number of receptors inside the nano-objects (Dani et al., 2010). Any NMDAR nano-object that was within 200 nm of PSD95 was considered localized at the synapse, whereas more distant nano-objects were considered extrasynaptic (Figures 2A and 2B). This distance cutoff was selected based on an estimation of the approximate size of the synapse using STORM images of Homer-1c (median Homer-1c width = 200 ± interquartile range [IQR] 141–287 nm, n = 622 synapses). Homer-1c is a synaptic structural reference (Figures S2A and S2B) (Dani et al., 2010) that co-localizes with 82% of PSD95 puncta in confocal images (Figures S2C and S2D). This analysis allowed us to distinguish and separately determine the synaptic and extrasynaptic populations of NMDARs.

Under control conditions, both the number of localizations within a nano-object and the size of the nano-objects were larger for those localized in synapses than those localized at extrasynaptic sites (mean number of localizations per nano-object ± SD = 129 ± 133 and 96 ± 95 and mean nano-object size ± SD = 35 ± 12 and 30 ± 10 nm for synaptic, n = 10,720, and extrasynaptic, n = 25,707, respectively) (Figure 2C; Figure S3A). These findings are expected considering the assembly of receptors at the synapse. We observed a slight variability in the nano-object size and the number of receptors per nano-object between control conditions in different experiments (Figure S3C). This variability is likely due to different patients' antibody batches used for labeling (Experimental Procedures) and small differences in the age of the neuronal cultures (17–21 days *in vitro*). Despite the small variability observed, incubation with different batches of patients' antibodies led to a consistent and substantial increase in both the size of the synaptic nano-objects and their relative receptor content starting at 2 hr (Figures 2C and 2D; Figures S3A–S3C). This initial increase was followed by a subsequent decline toward control values for 6–24 hr (Figures 2C and 2D; Figure S3A). The packing density of receptors inside the nano-objects also showed antibody-dependent changes, increasing above control levels (tight packing) at 2 hr and decreasing below control levels (loose packing) at 24 hr (Figure S3B).

Because our protocol involved labeling of NMDAR in live neurons, to ensure that potential secondary antibody cross-linking did not induce artifacts in the NMDAR nano-objects, we performed secondary antibody incubation using either live or fixed neurons to compare the NMDAR nano-object sizes.

Secondary antibodies only slightly increased the size of the NMDAR nano-objects in live neurons (mean nano-object size ± SD: 32 ± 10 nm, n = 4828) compared with fixed neurons (29 ± 9 nm, n = 4791). Therefore, the contribution of secondary antibodies to cross-linking of NMDAR nano-objects is minimal compared with the effects of patients' antibodies. Moreover, this small size change did not affect our findings, because all treatment conditions were equally affected (Figures 2C, 2D, and 3E; Figure S3).

Patients' Antibodies Preferentially Alter the Nanoscale Distribution of GluN2B-Containing Receptors

Previous studies showed that patients' antibodies altered differently the mobility of GluN2A- and GluN2B-containing receptors (Mikasova et al., 2012). To gain more insight into how NMDARs containing these subunits are organized at the nanoscale level and the effect of patients' antibodies on this organization, we quantified the antibody-mediated changes in the nanoscale distributions of GluN2A- and GluN2B-NMDAR using cultured rodent hippocampal neurons treated with patients' CSF antibodies for 24 hr.

We first assessed the change of cell-surface protein levels of GluN2A and GluN2B using immunoblot of biotinylated cell-surface proteins (Figure S4A). These studies showed a significant decrease of cell-surface GluN1, as well as GluN2A and GluN2B protein levels (Figure S4B). In parallel, we quantified with confocal microscopy the number of GluN2A and GluN2B puncta per unit length of dendrite (Figures 3A–3C). Consistent with western blot findings, there was a decrease in both the total and the synaptic density of NMDARs, regardless of their composition (Figures 3B and 3C). As previously reported using confocal microscopy (Hughes et al., 2010), these changes were not due to synaptic loss, because the density of PSD95 was unaffected (control CSF mean = 8.4 ± 2.3 puncta/unit length, n = 31 dendrites; patients' CSF mean = 7.6 ± 2.3 puncta/unit length, n = 41 dendrites). There was a greater reduction of GluN2B (79% and 87% reduction, $p < 0.0001$ for total and synaptic GluN2B, respectively) compared to GluN2A (55% and 38% reduction, $p < 0.0001$ and $p = 0.0059$ for total and synaptic GluN2A, respectively) (Figures 3A–3C), suggesting a different effect of the antibodies on the NMDAR subpopulations.

We next imaged GluN2A- and GluN2B-NMDAR subpopulations using STORM microscopy. These subunits were also organized in nano-objects, similar to the GluN1 subunit. As expected, both the GluN2A and the GluN2B nano-objects showed substantial co-localization with the obligatory GluN1 subunit (Figures S5A and S5C). This high co-localization was confirmed by NND analysis between GluN2A or GluN2B and GluN1 nano-objects (GluN2A to GluN1 NND median = 50 ± IQR 22–151 nm, n = 5,997; GluN2B to GluN1 NND median = 40 ± IQR 20–97 nm, n = 7,663) (Figures S5B and S5D). Under control conditions, the synaptic GluN2A nano-objects were substantially larger and contained more receptor localizations than their extra-synaptic counterparts (synaptic GluN2A mean number of localizations ± SD = 600 ± 602 localizations, n = 4,912; extrasynaptic GluN2A mean number of localizations ± SD = 451 ± 489 localizations, n = 9,312) (Figure 3E; Figure S5E). In contrast, the GluN2B nano-objects were more similar in size regardless of their localization (synaptic GluN2B mean number of localizations ± SD = 360 ± 462 localizations, n = 4,219; extrasynaptic GluN2B mean number of localizations ± SD = 307 ± 372 localizations, n = 7,938) (Figure 3E; Figure S5E). Furthermore, GluN2A nano-objects were larger overall compared to the GluN2B nano-objects (Figure 3E; Figure S5E). These results are consistent with the preferential occupancy of mature synapses by GluN2A-NMDARs (Flint et al., 1997; Hoffmann et al., 2000; Matta et al., 2011; Paoletti, 2011; Shi et al., 1997; Xing et al., 2006; Zhang and Sun, 2011). Treatment with patients' antibodies increased the size and the receptor content of the GluN2B nano-objects, whereas the size of the GluN2A nano-objects remained similar or slightly decreased compared to

control conditions (Figure 3E; Figure S5E). These subunit-specific effects were not due to differences in the patients' CSF used, given that the same CSF was used to determine the effects on each subunit. Overall, these findings show that despite a general reduction of surface NMDAR, the local synaptic reorganization caused by patients' antibodies occurs in a subunit-dependent manner, with the GluN2B subpopulation being preferentially affected. These findings are also in agreement with the greater antibody-induced reduction of GluN2B-NMDARs observed with confocal microscopy.

Treatment with Ephrin-B2 Antagonizes the Antibody-Induced Nanoscale Changes in the Surface Distribution of NMDAR

EphB2 is known to interact with NMDAR (Dalva et al., 2000). Previous studies showed that patients' antibodies disrupt this interaction and that activation of EphB2 by its ligand (ephrin-B2) antagonizes the antibody-induced receptor internalization, preventing the behavioral and memory deficits observed in an animal model of anti-NMDAR encephalitis (Planagumà et al., 2016). In addition, EphB2 activation prevented the antibody-induced alteration of NMDAR surface trafficking (Mikasova et al., 2012). To determine at the nanoscale level the effect of EphB2 activation on antibody-induced NMDAR changes, we used STORM imaging on neurons co-treated with patients' NMDAR antibodies and soluble ephrin-B2. Ephrin-B2 partially prevented the antibody-induced alterations in nano-object size and receptor content for both GluN1 and GluN2B subunits (Figures 2C, 2D, and 3E; Figures S3A, S3B, and S5E). This effect was already evident after 2 hr of co-treatment with patients' antibodies and ephrin-B2 (Figures 2C and 2D). These findings suggest that EphB2 activation prevents antibody-induced NMDAR clustering at the nanoscale level, which likely slows receptor internalization, keeping the surface receptor levels and receptor distribution.

Monte Carlo Simulations Recapitulate the Experimental Findings

To gain insight into the mechanisms behind these experimental observations, we carried out Monte Carlo simulations. Receptors were initially placed randomly in the synapse and extrasynaptic space according to our experimental observations (Experimental Procedures). Pockets of scaffold protein regions (SPRs) were randomly distributed in the synaptic and extrasynaptic surfaces. SPRs were assumed to act as sites of receptor clustering (Figure 4A) due to scaffold protein-receptor binding interactions. Such scaffold nanodomains have been observed in super-resolution images of PSD95 (Nair et al., 2013). The simulations were run for different times (2, 6, and 24 hr), and the surface distribution of receptors was determined at the end point. Receptors that were within 15 nm (roughly the experimental resolution) were considered to belong to a nano-object. The parameters of the simulation were optimized such that the receptors per nano-object remained constant over the different time points of the control simulation (Experimental Procedures; Video S1).

Simulation 1—To capture the receptor dynamics in the presence of patients' NMDAR antibodies, we took into account the occurrence of antibody-induced cross-linking by allowing nano-object formation whenever 2 or more receptors were within 9 nm of one another (approximate diameter of a receptor-antibody complex). Second, we implemented internalization of extrasynaptic nano-objects with a rate determined from the experimental data (Figures S6F–S6H; Supplemental Experimental Procedures). These two effects only

partially recapitulated the experimentally observed changes to NMDAR nano-objects in the presence of patients' antibodies (Figures S6B and S6C). With this simulation, the number of NMDARs inside the nano-objects initially increased and then decreased, similar to what was observed in the experiments. However, at 6 hr, there was still significant clustering of synaptic NMDARs above levels observed in the control simulation, contrary to experimental data. In addition, the extrasynaptic clustering was substantially higher than the synaptic clustering, which is opposed to the experimental results. Therefore, antibody-induced cross-linking and internalization alone could not fully capture the experimental results.

Simulation 2—Based on previous reports (Mikasova et al., 2012; Planagumà et al., 2016) and our data showing that activation of EphB2 antagonizes the effects of the antibodies, we hypothesized that the binding of antibodies to NMDAR leads to a disruption of its interaction with EphB2 and possibly other synaptic interacting partners. We thus increased by two-fold the unbinding rate of synaptic receptors from the SPR to reflect a potential disruption of receptor-protein interactions (Supplemental Experimental Procedures). This modification could recapitulate better the experimental observations at the synaptic level, but the amount of extrasynaptic NMDAR clustering remained inappropriately high compared with that of the synaptic NMDAR clustering (Figures S6D and S6E).

Simulation 3—Based on the preceding results, we hypothesized that interaction with proteins like EphB2 contributes to NMDAR dynamics not only at the synapse but also at the extrasynapse, albeit to a lesser extent, and that these interactions are disrupted by antibody binding. Therefore, we also increased the unbinding rate of extrasynaptic receptors from SPR. Compared with simulations 1 and 2, simulation 3 recapitulated better the experimental data on NMDAR nano-objects (Figure 4B; Videos S2 and S3) both inside and outside of the synapse, suggesting that NMDAR-protein interactions at both the synaptic and the extra-synaptic sites are important for NMDAR dynamics and account for the antibody-induced redistribution of surface NMDARs at the nanoscale level.

Using simulation 3, we also found that upon antibody treatment, more receptors were localized in the synapse compared to control simulation (Figure 4D). To experimentally validate this result, we quantified the observed percentage of synaptic and extrasynaptic NMDAR nano-objects under control conditions and after 24 hr of antibody treatment. In the analysis of the experimental data, the number of nano-objects was not normalized to the dendrite length. Because the total extrasynaptic length is larger than the synaptic length, the total number of experimentally determined extrasynaptic nano-objects appeared higher than the number of synaptic ones. Nonetheless, this analysis showed that the proportion of synaptic nano-objects increased with antibody treatment compared to control conditions and this effect could be partially antagonized with EphB2 activation (Figure 4E). Along with the total amount of surface NMDAR being significantly lower at this time point, the experimental and simulation results suggest that the remaining population of surface NMDAR is preferentially relocalized at the synapse. A different affinity of the receptors for SPR at the synapse compared with the extrasynaptic site seems to be crucial for this preferential retention of receptors at the synapse.

DISCUSSION

We previously reported that NMDAR antibodies from patients with anti-NMDAR encephalitis cause a decrease of cell-surface and synaptic NMDAR density, as well as total NMDAR protein in cultured hippocampal neurons (Hughes et al., 2010; Moscato et al., 2014). Additional studies showed that patients' antibodies alter the surface trafficking of NMDAR and that this effect is different depending on the GluN2 subunit composition (Mikasova et al., 2012). Here, we used super-resolution microscopy to determine the effect of patients' antibodies on the nanoscale distribution of synaptic and extrasynaptic NMDARs. Our findings show that NMDARs are normally organized into nano-objects, revealed by labeling both the GluN1 and the GluN2 subunits. These nano-objects are larger in the synapse than in the extrasynaptic spaces, and the synaptic GluN2A nano-objects are larger than the GluN2B nano-objects. These findings indicate an organization of the NMDARs at the nanoscale level that is subunit dependent. Such non-uniform enrichment of receptors into nanosized objects and domains has been previously reported for other synaptic proteins such as the AMPAR, for which nano-objects were visualized using both antibody labeling and fluorescent protein fusions (MacGillavry et al., 2013; Nair et al., 2013). In line with the studies on AMPAR, our findings support a model in which surface receptors are compartmentalized within the postsynaptic density, and this compartmentalization likely plays an important role in receptor physiology.

Previous studies using *in vitro* and *in vivo* models demonstrated that patients' CSF antibodies decrease the NMDAR surface and synaptic content and induce severe memory deficits (Hughes et al., 2010; Moscato et al., 2014; Planagumà et al., 2015). Recombinant human monoclonal NMDAR autoantibodies derived from patients' plasma cells had the same effects as those reported for patients' CSF antibodies (Malviya et al., 2017), indicating that the observed effects were caused by the antibodies, not by other CSF factors. Moreover, autoantibody-derived F(ab) (antigen binding) fragments did not decrease surface receptor density (Moscato et al., 2014), indicating that the cross-linking and internalization of NMDAR required the two arms of the antibody molecule and were not due to the labeling procedure. The current findings show that patients' antibodies caused an increased clustering of both synaptic and extrasynaptic NMDARs inside nano-objects, and these changes preceded receptor internalization (Figure 5). This antibody-induced receptor clustering likely triggers internalization once nano-objects reach a threshold size after approximately 2 hr of incubation with patients' antibodies. At later times, the sizes of the remaining surface nano-objects returned to control values, but the receptors were more loosely packed, having a lower density than those observed in control conditions (Figure 5). We found that antibodies preferentially clustered NMDARs containing GluN2B subunits. Previous studies showed that antibody treatment led to slower diffusion of GluN2B-containing NMDARs (Mikasova et al., 2012), which is consistent with the current super-resolution data in which GluN2B subunits became confined into larger nano-objects after antibody treatment. In the future, it would be interesting to determine the molecular mechanisms leading to subunit-specific reorganization of receptor nano-objects.

Antibody-induced clustering of proteins has been described using conventional microscopy in several pathological conditions (Harder et al., 1998; Mayor et al., 1994; Marta et al.,

2005); however, not all autoantibodies to synaptic receptors induce receptor aggregation. For example, in patients with another form of autoimmune encephalitis mediated by GABAb receptor antibodies, the antibodies do not cluster or internalize the cognate receptors (Dalmau et al., 2017). Using super-resolution microscopy, we could visualize the nanoscale organization of receptors and quantify the relative changes to the number of receptors in the nano-objects, which is not possible with conventional microscopy methods.

Monte Carlo simulations showed that NMDAR cross-linking by antibodies was not sufficient to explain the time course of changes affecting the NMDAR nano-objects. Simulations recapitulated the experimental observations taking into account four effects at the molecular level: (1) antibody-induced cross-linking of NMDARs, (2) increased rate of NMDAR internalization following receptor clustering, (3) disruption of NMDAR-protein interactions in the synapse, and (4) disruption of NMDAR-protein interactions at the extrasynaptic space. Consistent with these results, activation of EphB2 by its ligand ephrin-B2 antagonized the antibody-induced alterations of the NMDAR nano-scale distribution in both synaptic and extrasynaptic regions. An interesting prediction of the simulations was the antibody-induced relative increase of the density of synaptic versus extrasynaptic receptors, which was in line with the experimental findings. Our data suggest that differences in the strength of NMDAR-SPR interactions in synaptic and extrasynaptic spaces played an important role in this preferential relocalization of receptors at the synapse. It is likely that the interaction of NMDARs with several synaptic and extrasynaptic partners, in addition to EphB2 receptors, stabilizes NMDAR inside nano-objects and that patients' antibodies disrupt such interactions, explaining why EphB2 activation partially antagonizes the antibody effects. Based on these findings, a task for the future is to determine other interacting partners of NMDAR, the binding of which may also be disrupted by patients' antibodies. Intervention on these binding partners may have therapeutic implications similar to those experimentally demonstrated for EphB2 activation by ephrin-B2-like agonists (Mikasova et al., 2012; Planagumà et al., 2016).

EXPERIMENTAL PROCEDURES

Full details of the experimental procedures and analyses are provided online in the Supplemental Experimental Procedures.

Human CSF Samples and Animal Procedures

Samples of CSF from 5 patients with high-titer NMDAR antibodies (CSF+, determined according to previous studies; see Dalmau et al., 2008) were used on cultured neurons to determine the effects of patients' antibodies (Table S1). Samples of CSF from 5 subjects lacking NMDAR antibodies (CSF−) were used as controls (Table S1). Written consent for studies was obtained from patients or family members. Studies were approved by the institutional review board of Hospital Clínic and Institut d'Investigacions Biomèdiques August Pi i Sunyer (IDIBAPS), Universitat de Barcelona.

Primary hippocampal neurons were prepared from embryonic day (E) 18 embryos extracted from pregnant Wistar rats (Supplemental Experimental Procedures). Animal procedures

were conducted in accordance with standard ethical guidelines (European Communities Directive 86/609/EU) and approved by the local ethical committees.

Sample Preparation and STORM Imaging

Primary hippocampal neurons that had been cultured for 17–21 days *in vitro* were treated with either control or patients' CSF for 2, 6, or 24 hr in the presence or absence of ephrin-B2 (0.5 $\mu g.mL^{-1}$). Surface proteins were labeled by incubating live cells for 30 min at 37°C with primary antibodies and then with the corresponding secondary antibodies labeled with the Alexa Fluor 405-Alexa Fluor 647 dye pair for 30 min at 37°C. Synaptic markers were labeled after fixation and permeabilization steps by incubating cells for 1 hr at room temperature (RT) with the corresponding primary antibodies and another 1 hr of incubation at RT with a corresponding secondary antibody prepared for STORM imaging.

All imaging experiments were carried out with a commercial STORM microscope system from Nikon Instruments (NSTORM). For single-color imaging, 647 nm laser light was used for exciting the reporter dye (Alexa Fluor 647, Invitrogen) and switching it to the dark state, and 405 nm laser light was used for reactivating the Alexa Fluor 647 into a fluorescent state in an activator dye (Alexa Fluor 405)-facilitated manner. Dual-color imaging was performed with two sets of secondary antibodies labeled with the same reporter dye (Alexa Fluor 647) but two activator dyes (Alexa Fluor 405 and Cy3) (Bates et al., 2007). The emitted light was collected by an oil immersion 100×, 1.49 numerical aperture (NA) objective; filtered by an emission filter (ET705/72 m); and imaged onto an electron-multiplying charge-coupled device (EMCCD) camera at an exposure time of 20 ms per frame.

STORM Data Analysis

The final images were rendered by representing each x-y position (localization) as a Gaussian with a width that corresponds to the determined localization precision (9 nm). Sample drift during acquisition and crosstalk between the imaging channels were accounted for and corrected (Huang et al., 2008), and a cluster analysis algorithm previously developed in the team (Ricci et al., 2015) was used to group localizations in nano-objects (Supplemental Experimental Procedures). Nano-objects' sizes were calculated as the SD of localization coordinates from the relative nano-object centroid.

Monte Carlo Simulations

Details of the simulations can be found in Supplemental Experimental Procedures.

Statistics

Confocal spot densities of GluN1 and PSD95 were analyzed using one-way ANOVA and post hoc testing with Tukey adjustment for multiple comparisons. Confocal spot densities of GluN2A and GluN2B were analyzed using the t test with Welch's correction. Quantitative immunoblot data were analyzed using the t test with Welch's correction.

STORM nano-object properties, following a non-normal distribution, were analyzed using non-parametric statistics. The Mann-Whitney test was used for pair comparisons, while the

Kruskal-Wallis test, followed by post hoc testing with Dunn's correction, was applied for multiple comparisons.

A p value inferior to 0.05 was considered significant. All tests were done using GraphPad Prism v.6 (GraphPad, La Jolla, CA, USA).

Supplementary Material

Refer to Web version on PubMed Central for supplementary material.

Acknowledgments

We thank all members of the Advanced Fluorescence Imaging and Biophysics group (Institute of Photonic Sciences [ICFO], Barcelona), L. Groc (University of Bordeaux), and A.L. Carvalho (University of Coimbra) for critical reading of the manuscript and helpful discussions. We thank B. Huang (University of California, San Francisco [UCSF]) for Insight3 STORM analysis software. We thank M. Rivas Jiménez (Institute of Photonic Sciences [ICFO], Barcelona) for her technical support with cell cultures. We thank P. Relich (University of Pennsylvania) for his help with the video illustrations. We thank A. Hirschmann (Institute of Photonic Sciences [ICFO], Barcelona) for her help in designing the graphical abstract. We acknowledge the ICFO Super-resolution Light Nanoscopy (SLN) facility and the ICFO Nikon Center of Excellence in STORM. This work was supported by Instituto Carlos III/FEDER PIE 16/00014, CIBERER 15/00010, NIH RO1NS077851, Generalitat de Catalunya AGAUR SGR93, and Fundació CELLEX (M.L. and J.D.); the European Commission's Marie Curie Actions for Co-funding of Regional, National and International Programmes (COFUND); and the Spanish Ministry of Economy and Competitiveness (MINECO) (L.L.).

References

Bates M, Huang B, Dempsey GT, Zhuang X. Multicolor super-resolution imaging with photo-switchable fluorescent probes. Science. 2007; 317:1749–1753. [PubMed: 17702910]

Dalmau J, Graus F. Antibody-Mediated Encephalitis. N Engl J Med. 2018; 378:840–851. [PubMed: 29490181]

Dalmau J, Gleichman AJ, Hughes EG, Rossi JE, Peng X, Lai M, Dessain SK, Rosenfeld MR, Balice-Gordon R, Lynch DR. Anti-NMDA-receptor encephalitis: case series and analysis of the effects of antibodies. Lancet Neurol. 2008; 7:1091–1098. [PubMed: 18851928]

Dalmau J, Geis C, Graus F. Autoantibodies to Synaptic Receptors and Neuronal Cell Surface Proteins in Autoimmune Diseases of the Central Nervous System. Physiol Rev. 2017; 97:839–887. [PubMed: 28298428]

Dalva MB, Takasu MA, Lin MZ, Shamah SM, Hu L, Gale NW, Greenberg ME. EphB receptors interact with NMDA receptors and regulate excitatory synapse formation. Cell. 2000; 103:945–956. [PubMed: 11136979]

Dani A, Huang B, Bergan J, Dulac C, Zhuang X. Superresolution imaging of chemical synapses in the brain. Neuron. 2010; 68:843–856. [PubMed: 21144999]

Dupuis JP, Ladépêche L, Seth H, Bard L, Varela J, Mikasova L, Bouchet D, Rogemond V, Honnorat J, Hanse E, Groc L. Surface dynamics of GluN2B-NMDA receptors controls plasticity of maturing glutamate synapses. EMBO J. 2014; 33:842–861. [PubMed: 24591565]

Flint AC, Maisch US, Weishaupt JH, Kriegstein AR, Monyer H. NR2A subunit expression shortens NMDA receptor synaptic currents in developing neocortex. J Neurosci. 1997; 17:2469–2476. [PubMed: 9065507]

Gleichman AJ, Spruce LA, Dalmau J, Seeholzer SH, Lynch DR. Anti-NMDA receptor encephalitis antibody binding is dependent on amino acid identity of a small region within the GluN1 amino terminal domain. J Neurosci. 2012; 32:11082–11094. [PubMed: 22875940]

Harder T, Scheiffele P, Verkade P, Simons K. Lipid domain structure of the plasma membrane revealed by patching of membrane components. J Cell Biol. 1998; 141:929–942. [PubMed: 9585412]

Hoffmann H, Gremme T, Hatt H, Gottmann K. Synaptic activity-dependent developmental regulation of NMDA receptor subunit expression in cultured neocortical neurons. J Neurochem. 2000; 75:1590–1599. [PubMed: 10987840]

Huang B, Wang W, Bates M, Zhuang X. Three-dimensional super-resolution imaging by stochastic optical reconstruction microscopy. Science. 2008; 319:810–813. [PubMed: 18174397]

Hughes EG, Peng X, Gleichman AJ, Lai M, Zhou L, Tsou R, Parsons TD, Lynch DR, Dalmau J, Balice-Gordon RJ. Cellular and synaptic mechanisms of anti-NMDA receptor encephalitis. J Neurosci. 2010; 30:5866–5875. [PubMed: 20427647]

MacGillavry HD, Song Y, Raghavachari S, Blanpied TA. Nanoscale scaffolding domains within the postsynaptic density concentrate synaptic AMPA receptors. Neuron. 2013; 78:615–622. [PubMed: 23719161]

Malviya M, Barman S, Golombeck KS, Planagumà J, Mannara F, Strutz-Seebohm N, Wrzos C, Demir F, Baksmeier C, Steckel J, et al. NMDAR encephalitis: passive transfer from man to mouse by a recombinant antibody. Ann Clin Transl Neurol. 2017; 4:768–783. [PubMed: 29159189]

Marta CB, Montano MB, Taylor CM, Taylor AL, Bansal R, Pfeiffer SE. Signaling cascades activated upon antibody cross-linking of myelin oligodendrocyte glycoprotein: potential implications for multiple sclerosis. J Biol Chem. 2005; 280:8985–8993. [PubMed: 15634682]

Matta JA, Ashby MC, Sanz-Clemente A, Roche KW, Isaac JTR. mGluR5 and NMDA receptors drive the experience- and activity-dependent NMDA receptor NR2B to NR2A subunit switch. Neuron. 2011; 70:339–351. [PubMed: 21521618]

Mayor S, Rothberg KG, Maxfield FR. Sequestration of GPI-anchored proteins in caveolae triggered by cross-linking. Science. 1994; 264:1948–1951. [PubMed: 7516582]

Mikasova L, De Rossi P, Bouchet D, Georges F, Rogemond V, Didelot A, Meissirel C, Honnorat J, Groc L. Disrupted surface crosstalk between NMDA and Ephrin-B2 receptors in anti-NMDA encephalitis. Brain. 2012; 135:1606–1621. [PubMed: 22544902]

Moscato EH, Peng X, Jain A, Parsons TD, Dalmau J, Balice-Gordon RJ. Acute mechanisms underlying antibody effects in anti-N-methyl-D-aspartate receptor encephalitis. Ann Neurol. 2014; 76:108–119. [PubMed: 24916964]

Nair D, Hosy E, Petersen JD, Constals A, Giannone G, Choquet D, Sibarita JB. Super-resolution imaging reveals that AMPA receptors inside synapses are dynamically organized in nanodomains regulated by PSD95. J Neurosci. 2013; 33:13204–13224. [PubMed: 23926273]

Oddone A, Vilanova IV, Tam J, Lakadamyali M. Super-resolution imaging with stochastic single-molecule localization: concepts, technical developments, and biological applications. Microsc Res Tech. 2014; 77:502–509. [PubMed: 24616244]

Paoletti P. Molecular basis of NMDA receptor functional diversity. Eur J Neurosci. 2011; 33:1351–1365. [PubMed: 21395862]

Pennacchietti F, Vascon S, Nieus T, Rosillo C, Das S, Tyagarajan SK, Diaspro A, Del Bue A, Petrini EM, Barberis A, Cella Zanacchi F. Nanoscale Molecular Reorganization of the Inhibitory Postsynaptic Density Is a Determinant of GABAergic Synaptic Potentiation. J Neurosci. 2017; 37:1747–1756. [PubMed: 28073939]

Planagumà J, Leypoldt F, Mannara F, Gutiérrez-Cuesta J, Martín-García E, Aguilar E, Titulaer MJ, Petit-Pedrol M, Jain A, Balice-Gordon R, et al. Human N-methyl D-aspartate receptor antibodies alter memory and behaviour in mice. Brain. 2015; 138:94–109. [PubMed: 25392198]

Planagumà J, Haselmann H, Mannara F, Petit-Pedrol M, Grünewald B, Aguilar E, Röpke L, Martín-García E, Titulaer MJ, Jercog P, et al. Ephrin-B2 prevents N-methyl-D-aspartate receptor antibody effects on memory and neuroplasticity. Ann Neurol. 2016; 80:388–400. [PubMed: 27399303]

Ricci MA, Manzo C, García-Parajo MF, Lakadamyali M, Cosma MP. Chromatin fibers are formed by heterogeneous groups of nucleosomes *in vivo*. Cell. 2015; 160:1145–1158. [PubMed: 25768910]

Rust MJ, Bates M, Zhuang X. Sub-diffraction-limit imaging by stochastic optical reconstruction microscopy (STORM). Nat Methods. 2006; 3:793–795. [PubMed: 16896339]

Shi J, Aamodt SM, Constantine-Paton M. Temporal correlations between functional and molecular changes in NMDA receptors and GABA neurotransmission in the superior colliculus. J Neurosci. 1997; 17:6264–6276. [PubMed: 9236237]

Specht CG, Izeddin I, Rodriguez PC, El Beheiry M, Rostaing P, Darzacq X, Dahan M, Triller A. Quantitative nanoscopy of inhibitory synapses: counting gephyrin molecules and receptor binding sites. Neuron. 2013; 79:308–321. [PubMed: 23889935]

Xing GG, Wang R, Yang B, Zhang D. Postnatal switching of NMDA receptor subunits from NR2B to NR2A in rat facial motor neurons. Eur J Neurosci. 2006; 24:2987–2992. [PubMed: 17156360]

Zhang Z, Sun QQ. Development of NMDA NR2 subunits and their roles in critical period maturation of neocortical GABAergic interneurons. Dev Neurobiol. 2011; 71:221–245. [PubMed: 20936660]

Highlights

- NMDARs form nano-objects on the neuronal surface
- Autoantibodies increase NMDAR nano-object size and content before internalization
- Cross-linking and disruption of NMDAR-protein interactions cause increased clustering
- EphB2 receptor activation antagonizes the antibody effects on NMDAR nano-organization

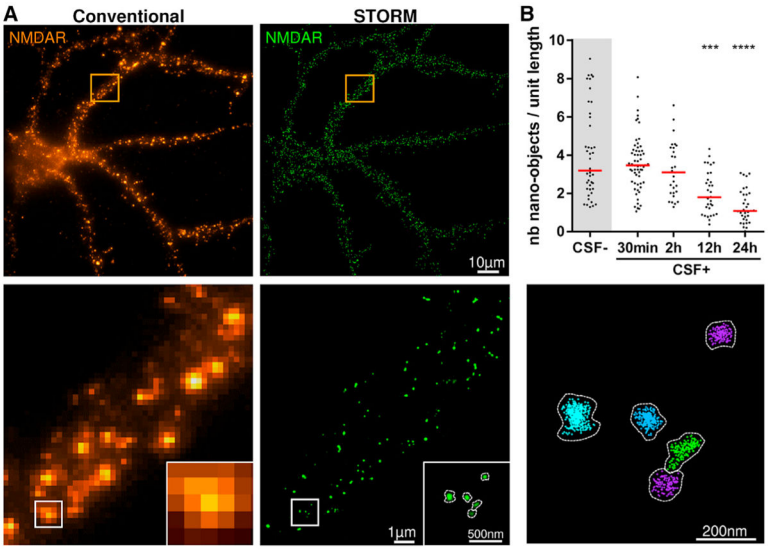

Figure 1. NMDAR Autoantibodies Lead to a Decrease in the Surface Density of NMDAR Nano-objects as Revealed by Super-resolution Microscopy

(A) A representative conventional wide-field (upper left panel) and super-resolution (upper right panel) fluorescence image of NMDAR in cultured hippocampal neurons. Zoom of the region inside the orange square in the conventional image is shown in the lower left panel. A super-resolution image of the region inside the white square is shown in the lower middle panel. The lower right panel displays the result of the cluster analysis, in which each NMDAR nano-object in the super-resolution image is segmented as a different color using the raw localization data. The number of localizations (given by the individual crosses), the area of the nano-objects, and the number of localizations per nano-object can be quantified after cluster analysis.

(B) Neurons were treated for 30 min or 2, 6, 12, or 24 hr with control or patients' CSF (CSF − and CSF+, respectively), and the density of surface NMDAR nano-objects per unit length (in micrometers) of dendrite was measured in the super-resolution images. When compared to control CSF (CSF−), the incubation with patients' CSF (CSF+) caused a significant reduction of the surface NMDAR nano-objects, with a maximal reduction at 24 hr of treatment. Bars represent medians, and dots correspond to individual cells ($n \geq 29$ fields of view; ***$p < 0.001$, ****$p < 0.0001$).

See also Figures S1 and S2.

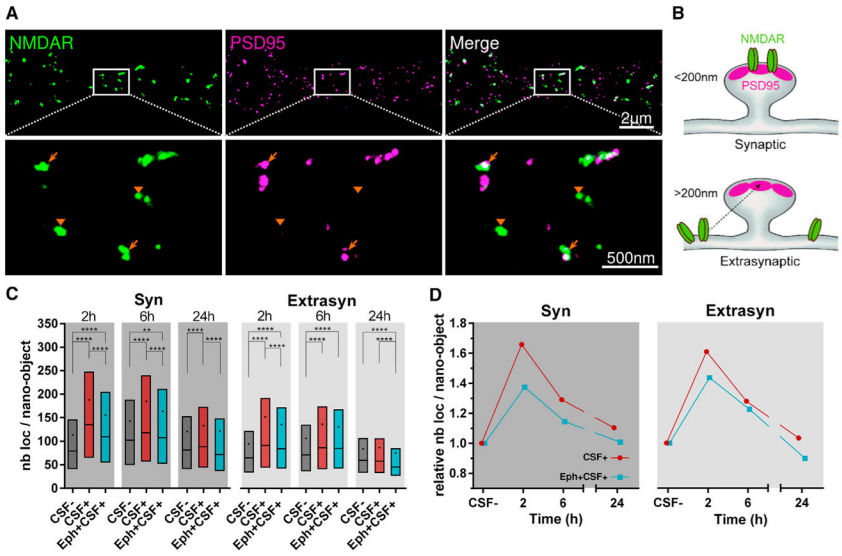

Figure 2. NMDAR Autoantibodies Induce a Time-Dependent Increase in the Receptor Content of the Surface NMDAR Nano-objects

(A) Upper panels show a representative STORM image of the surface NMDAR (green) and PSD95 (magenta). Lower panels are higher magnifications of the white region, showing examples of synaptic (arrows) and extrasynaptic (arrowheads) NMDAR nano-objects.

(B) Schematic illustration representing the distinction used to identify synaptic versus extrasynaptic NMDAR nano-objects located within 200 nm of the center of the closest PSD95 nano-object versus farther away.

(C) Quantification of the number of localizations per NMDAR nano-object, a relative measure of the receptor content of the nano-objects, after 2, 6, or 24 hr of incubation with the control CSF (CSF−, dark gray), with patients' CSF alone (CSF+, red), or in the presence of ephrin-B2 (Eph+CSF+, cyan). The box, line, and dot correspond to interquartile range (IQR, 25^{th}–75^{th} percentile), median, and mean, respectively (synaptic, n ≥ 835 nano-objects; extrasynaptic, n ≥ 2001 nano-objects; **p < 0.01, ***p < 0.001, ****p < 0.0001).

(D) Relative change in the number of localizations per nano-object obtained by normalizing the CSF+ means at each time to the corresponding CSF− means.

(See also Figure S3.

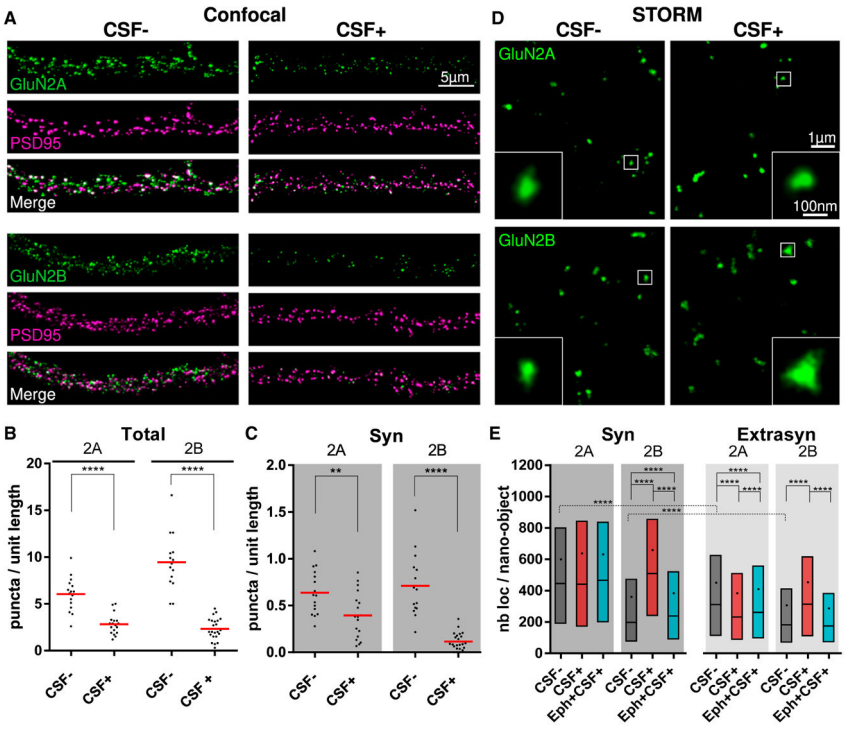

Figure 3. NMDAR Autoantibodies Alter Differently the Distribution of GluN2A-NMDAR and GluN2B-NMDAR

(A) Representative confocal images of surface GluN2A-NMDAR (green, upper panels) or GluN2B-NMDAR (green, lower panels) subunits labeled, together with PSD95 (magenta), after 24 hr of incubation of control or patients' CSF (CSF−, left panels, and CSF+, right panels). Note the visible decrease in the GluN2A and GluN2B labeling in the presence of the patients' CSF.

(B and C) Quantification of the density of surface GluN2A or GluN2B puncta per unit length (in micrometers) of dendrite either considering all surface puncta (B, Total) or isolating the ones that co-localize with PSD95, and are synaptic (C, Syn). Red lines represent the means, and dots correspond to individual cells ($n \geq 15$ fields of view; $^{**}p < 0.01$, $^{***}p < 0.001$, $^{****}p < 0.0001$).

(D) Representative STORM images of GluN2A (upper) and GluN2B (lower) that have been incubated with control or patients' CSF (CSF−, left panels, and CSF+, right panels, respectively) for 24 hr. Insets show zooms of nano-objects corresponding to the white squared region. Note the increased size of the GluN2B nano-objects in the CSF+ condition.

(E) Quantification of the number of localizations per NMDAR nano-object after 24 hr of incubation with control CSF (CSF−, dark gray), with patients' CSF alone (CSF+, red), or in the presence of ephrin-B2 (Eph+CSF+, cyan). The box, line, and dot correspond to IQR, median, and mean, respectively (synaptic, $n \geq 2{,}649$ nano-objects; extrasynaptic, $n \geq 5{,}213$ nano-objects; $^{****}p < 0.0001$).

See also Figures S4 and S5.

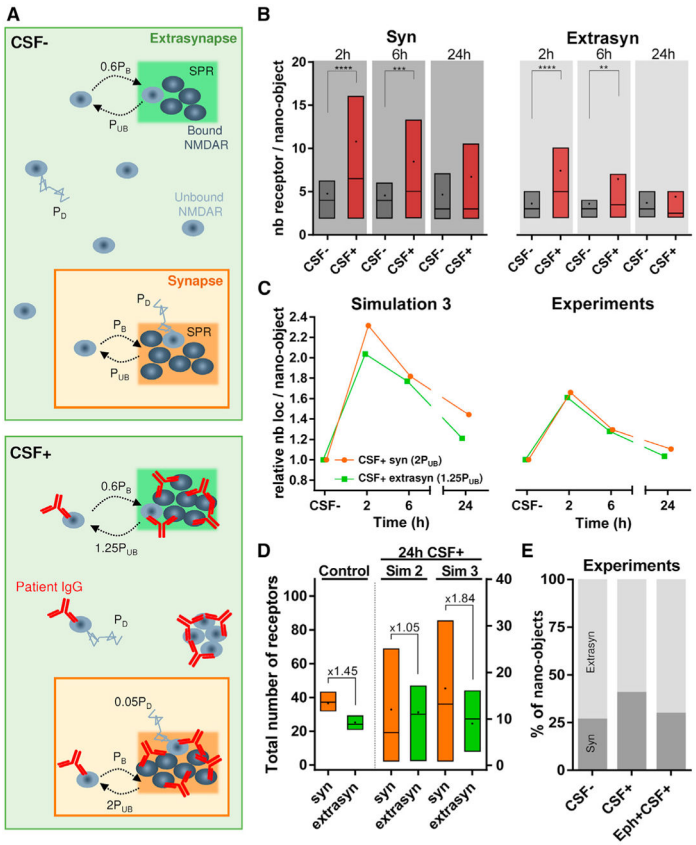

Figure 4. Monte Carlo Simulations Recapitulate Experimental Results

(A) Schematic representation (top view) of NMDAR dynamics simulation for CSF− (control or without antibodies) and CSF+ (with NMDAR antibodies). The synapse and extrasynapse are represented as orange and green areas, respectively (not represented here at their true scale value), with one scaffold protein region (SPR) in each. The receptors follow binding and unbinding events with the scaffold proteins in the SPR and can be in a bound state (dark gray) or an unbound state (light gray). The binding probability of a receptor is $P_B = 1$ in the synapse and $0.6P_B$ in the extra-synapse for both CSF− and CSF+. The unbinding probability of a receptor is $P_{UB} = 0.167$ in both the extrasynapse and the synapse for CSF−. For CSF+, unbinding probability increases to $1.25P_{UB}$ in the extrasynapse and $2P_{UB}$ in the synapse. All unbound receptors diffuse with a probability $P_D = 1$ for CSF−. For CSF+, unbound receptors belonging to a nano-object diffuse with a reduced probability of $0.05P_D$, but this diffusion probability remains unchanged for unbound receptors not forming any nano-object.

(B) Distribution of receptors per nano-object at 2, 6, and 24 hr in the synapse and extrasynapse for both CSF− and CSF+ conditions obtained from simulation. The box, line, and dot correspond to IQR, median, and mean, respectively (synaptic, $n \geq 56$ nano-objects; extrasynaptic, $n \geq 60$ nano-objects; **$p < 0.01$, ***$p < 0.001$, ****$p < 0.0001$). (C) Comparison of the fold change in nano-object content at different times (2, 6, and 24 hr) relative to the corresponding CSF− values for simulations (left) and experimental data (right). Each data point is obtained by normalizing the mean of receptors per nano-object value at each time point for CSF+ with the mean of receptors per nano-object value obtained from the corresponding time points for CSF−.

(D) Total number of receptors present in the synapse (orange) and extrasynapse (green) at 24 hr for simulation control (left), simulation 2 (middle), and simulation 3 (right). Data are obtained from the simulated area of ~200 × 200 nm^2 for both synapse and extrasynapse. The fold difference from the mean of the synaptic to the extrasynaptic number of receptors is indicated above the boxes. The box, line, and dot correspond to IQR, median, and mean, respectively (control, n = 40 runs; simulation 2, n = 19 runs; simulation 3, n = 22 runs).
(E) Quantification of percentage of synaptic (dark gray) versus extrasynaptic (light gray) nano-objects from experimental data after 24 hr of treatment with patients' CSF alone (CSF +) or in the presence of ephrin-B2 (Eph+CSF+).
See also Figure S6 and Videos S1, S2, and S3.

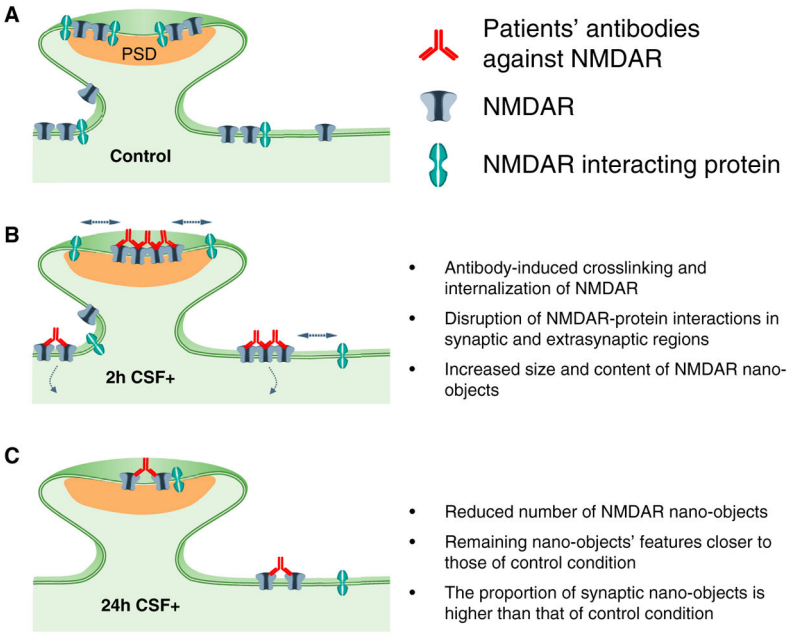

Figure 5. Schematic Representation of the Changes Occurring in NMDAR Organization following Treatment with Patients' NMDAR Antibodies

(A) Under control conditions, NMDAR are distributed at the neuronal surface, forming nano-objects both inside and outside the synapse.

(B) At early times, antibody-induced clustering leads to formation of larger nano-objects containing more receptors, particularly in the synapse.

(C) At later times, dynamic exchange of receptors, facilitated by the disruption of NMDARs' interaction with other proteins in both the synapse and the extrasynapse, coupled with clustering-induced internalization, leads to a decrease in NMDAR nano-object size and content back toward control values while leading to an overall global decrease of NMDAR nano-objects.